Earthq Eng & Eng Vib (2011) 10: 325-337 **DOI**: 10.1007/s11803-011-0069-x

Improved HVSR site classification method for free-field strong motion stations validated with Wenchuan aftershock recordings

Wen Ruizhi[1†], Ren Yefei [‡] and Shi Dacheng[‡]

Institute of Engineering Mechanics, China Earthquake Administration, Harbin 150080, China

Abstract: Local site conditions play an important role in the effective application of strong motion recordings. In the China National Strong Motion Observation Network System (NSMONS), some of the stations do not provide borehole information, and correspondingly, do not assign the site classes yet. In this paper, site classification methodologies for free-field strong motion stations are reviewed and the limitations and uncertainties of the horizontal-to-vertical spectral ratio (HVSR) methods are discussed. Then, a new method for site classification based on the entropy weight theory is proposed. The proposed method avoids the head or tail joggle phenomenon by providing the objective and subjective weights. The method was applied to aftershock recordings from the 2008 Wenchuan earthquake, and 54 free-field NSMONS stations were selected for site classification and the mean HVSRs were calculated. The results show that the improved HVSR method proposed in this paper has a higher success rate and could be adopted in NSMONS.

Keywords: site classification; strong motion recording; entropy weight theory; horizontal-to-vertical spectrum ratio; Wenchuan earthquake aftershock; head-tail joggle

1 Introduction

Local site conditions have a significant influence on ground motion characteristics and seismic performance of engineering structures. Different site conditions may induce varied amplification of the ground motion leading to abnormal earthquake damage phenomenon (Hu *et al*., 1980; Zhou, 1990; China Earthquake Investigation Group Aboard to Japan, 1995; Li, 1996). It was observed from the 1906 San Francisco earthquake that the most important characteristics of the strong motion showed that there was a clear correlation between the earthquake intensity of a site and its underlying geologic conditions. Wood (1908) found that the variability of the surface geology in the San Francisco Bay area contributed the most the significant change in the strong motion characteristics during their site investigation. Subsequent earthquakes, such as the 1923 Great Kanto earthquake (Ohsaki, 1969), 1976 Tangshan earthquake (Gao and Hu, 1987; Liu and Cha, 1982), 1985 Mexico earthquake (Seed *et al*., 1988), 1999 Chi-Chi earthquake (Tsai and Huang, 2000), and the recent 2008 Wenchuan earthquake (Bo *et al*., 2009) have all validated the important effects of the site conditions on building damage. The concept of site classification has been gradually incorporated in seismic codes in many countries. The February 27, 2010 Chile earthquake supported this knowledge of site classifications in an interesting way. An investigation found that two similar buildings located 20 m apart near the Llacolen bridge in downtown Concepcion were impacted in completely different ways: one was destroyed and the other suffered only minor damage. Their proximity excludes the effects of the soil conditions, and this abnormal occurrence may be attributed to the site classification used in design. The destroyed building was designed using Site Type II, while the other was designed using Site Type III (GEER Association Team, 2010).

Strong motion recordings are widely used in investigations and engineering practice, such as seismic zonation, seismic risk analysis and earthquake resistant design, and response analyses of buildings, among others. In recent years, strong motion data have become more available from a diverse array of organizations and services. High quality strong motion recordings are not just a set of qualified accelerograms, but also include station location, earthquake data sources, ground motion parameters, and other information pertaining to the particular recording. Site classification of a strong motion station is one of the parameters required to determine the suitability of its recordings for specific applications.

Correspondence to: Wen Ruizhi, Institute of Engineering Mechanics, China Earthquake Administration, Harbin 150080, China
Tel: 86-0451-86652617; Fax: 86-0451-86664755
E-mail: ruizhi@iem.net.cn
[†]Professor; [‡]PhD Candidate

Supported by: National Key Technology R & D Program Under Grant No. 2009BAK55B05; Nonprofit Industry Research Project of CEA Under Grant No. 201108003; Science Foundation of Institute of Engineering Mechanics, CEA Under Grant No. 2010C01
Received March 21, 2011; **Accepted** August 2, 2011

The China National Strong Motion Observation Network System (NSMONS) was deployed in 2008. During the M_s8.0 Great Wenchuan earthquake, more than 1,400 high-quality strong motion recordings were obtained (Li *et al*., 2008), and then more than 2,000 sets of 3-channel strong motion recordings were obtained from 383 aftershocks. After the mainshock, another 59 strong ground motion instruments were temporarily installed along the Longmenshan Fault region, and more than 3,250 sets of 3-channel recordings were collected from the aftershocks. All these data enriched the Chinese strong motion database (Li, 2009). In China, standard strong motion recording processing includes a review and processing to reduce random noise in the recorded signals; it does not include site classification information. For NSMONS, some stations do not have adequate borehole information, so no site classification has been assigned for these stations. According to the Chinese seismic code, the borehole profile is usually to 20 m depth and the average shear-wave velocity is calculated from the top soil layer of 20 m depth (V_s^{20}). The average shear-wave velocity from the surface to 30 m depth (V_s^{30}) is now adopted as an international standard for site classification. Wen *et al*. (2010) provided the site classifications of 77 near-fault stations by using the HVSR method and the response spectral shapes (RSS) method. These classifications were based only on the recordings from Wenchuan mainshock, and as a result, they lack reliability. In this paper, an improved HVSR method is suggested and applied to 54 free-field strong motion stations considering the recordings from the Wenchuan earthquake aftershocks.

2 Site classification schemes

2.1 Development of HVSR schemes

The HVSR method was first proposed by Nakamura (1989), who used a horizontal-to-vertical Fourier spectrum ratio of interest ground microtremor to evaluate the site characteristics. Yamazaki and Ansary (1997) extended this method to earthquake ground motion recordings to compute horizontal-to-vertical Fourier spectrum ratios. They found that it was a stable method, regardless of the ground shaking level, station-to-source distance, and top soil layer depth, and could be a useful tool for site condition evaluation.

Lee *et al*. (2001) used a scheme compatible with the 1997 UBC provisions to classify 708 free-field strong motion station sites obtained from the Taiwan Strong-motion Instrumentation Program (TSMIP), in which the RSS method and HVSR method were both used for verification purposes. Their results have since been widely cited by researchers in engineering seismology (Hwang *et al*., 2004; Sokolov *et al*., 2002, 2003; Liu and Tsai, 2005; Lin and Lee, 2008; Roumelioti and Beresnev, 2003). Zare *et al*. (1999) provided free-field station classifications for the Iran strong motion network. Zhao *et al*. (2006) used *H/V* ratios for records from the classified *K*-net sites to establish a site classification index using mean spectral ratios over a wide range of spectral periods. Fukushima *et al*. (2007) suggested that HVSR was an effective method when borehole data was unavailable. After the Chi-Chi earthquake, the Center for Research in Earthquake Engineering (NCREE) and Weather Bureau (CWB*)* of Taiwan completed borehole measurement and provided PS logging data for 439 strong motion stations from 2000 to 2010. Then, Lee and Tsai (2008) combined the Geo2005 drilling database of the Geological Survey (CGS) of Taiwan to evaluate V_s^{30} values for each grid-point, and completed a V_s^{30} map of Taiwan. The strong motion data from two Pingtung, Taiwan, earthquakes that occurred on December 26, 2006, showed that ground motions on soil sites are generally larger than those on rock sites.

In the Next Generation Attenuation (NGA) research project, metadata characterizing each recording was developed that included the station site classification and V_s^{30}, and the improved data quality was made available for ground motion research and engineering practice (Chiou *et al*., 2008).

Ghasemi *et al.* (2009) improved the practicality and efficiency of the HVSR method introduced by Zhao *et al.* (2006) through Spearman rank technology. Garniel *et al*. (2008, 2009) improved this method with a wavelet analysis and self-organizing map method to more efficiently determine the predominant frequency.

2.2 HVSR classification schemes (Japan Road Association, 1980)- Method 1

Table 1 lists the site class definition used in the Japan earthquake resistant design code, together with the approximately corresponding National Earthquake Hazard Reduction Program (NEHRP) site classes. The site natural period as a key index of the site classification can be approximately obtained from the HVSR curves. Figure 1 illustrates the empirical HVSR curves plotted by Zhao *et al*. (2006) for four site classes.

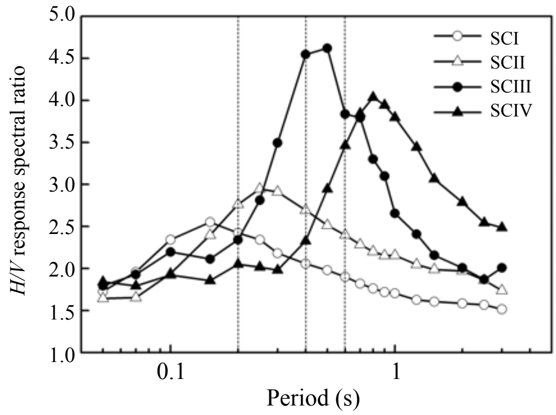

Fig. 1 Mean HVSR plots for different site classes (Zhao *et al*., 2006). The vertical dashed lines represent the bounds of two adjacent site classes provided in Table 1

Table 1 Site class definition used in Japan earthquake resistant design code and the approximately corresponding NEHRP site class (Japan Road Association, 1980)

Site class	Site natural period (s)	Average shear wave velocity (m·s^{-1})	NEHRP class
SC I: (Rock/stiff soil)	$T_G < 0.2$s	$V_s^{30} > 600$m/s	A+B
SC II: (Hard soil)	$0.2\text{s} \le T_G < 0.4$s	$300\text{m/s} < V_s^{30} \le 600$m/s	C
SC III: (Medium soil)	$0.4\text{s} \le T_G < 0.6$s	$200\text{m/s} < V_s^{30} \le 300$m/s	D
SC IV: (Soft soil)	$T_G \ge 0.6$s	$V_s^{30} \le 200$m/s	E

Note: T_G : Site natural period; V_s^{30} : Average shear wave velocity of 30m surface soil layer

When there are many recordings at a station, peak periods from the HVSR plot can be used to easily identify the site natural period, and as the number of recordings decreases, the accuracy also decreases rapidly (Zhao *et al*., 2004). The shortcoming of using a single index is that it is difficult to identify the site natural period if the HVSR curve has multiple similar peak periods as indicated by Ghasemi *et al*. (2009), who provided an example from the Rezvanshahr station in Iran strong motion network. They completed a successful identification for SC I, SC II, and SC III, and found that only 57%, 43% and 42%, respectively, and the low efficiency also manifested at Japanese K-net (Zhao *et al*., 2006). Zhao *et al.* (2006) suggested that this method could be appropriate for SC IV and SC III, but was unreliable for SC I and SC II. For SC IV and SC III, namely soft soil, the long period component is amplified well. However, for SC I and SC II, it is usually not possible to choose the peak period at high frequency, so the site class is ambiguous .

2.3 HVSR classification schemes (Zhao *et al*., 2006)-Method 2

Zhao *et al*. (2006) suggested an index classification considering peak period and the *H/V* spectral ratios at all periods to improve the accuracy of the previous scheme as follows:

$$\mathrm{SI}_k = \frac{2}{n}\sum_{i=1}^{n} F\left(-\mathrm{abs}\left[\ln\left(\mu_i\right) - \ln\left(\bar{\mu}_{ki}\right)\right]\right) \tag{1}$$

where k is the site class number, n is the total number of periods, $F()$ is the normal cumulative distribution function, μ_i is the mean *H/V* ratio for the ith period of the interest site, and $\bar{\mu}_{ki}$ is the standard *H/V* ratio for the ith period with respect to the kth site class. The success rate for SC I, SC III and SC IV is improved but is still only 30%–40% for SC II. Ghasemi *et al*. (2009) arrived at a similar conclusion with data from the Iran strong motion network.

Following a detailed analysis, it can be stated that there are two reasons that contribute to this low accuracy. First, this method is essentially based on the standard shape of *H/V* ratios. The standard shape is actually the geometric meaning of selected strong motion recordings, so the standard deviation should have been included. Second, from Eq.(1), the SI value expresses the similarity of the specific station *H/V* ratio shape to match the standard shape. For each period, the contribution to SI is equal. Actually, the peak period and its adjacent ones should have a higher contribution to SI. In order to provide a detailed explanation, three scenario HVSR curves are constructed and are shown in Fig. 2.

In Fig. 2, the scenario HVSR curve A has an obvious peak value at 0.3 s, and the segment at 0.2–0.4 s is close to the standard SC II curve; thus, the ideal result should be SC II. In Method 2, the site should belong to SC I from Table 2. This is attributed to Curve A being too close to the standard SCI curve at periods between <0.15 s and >0.7 s; this is called the head-tail joggle phenomenon. Ideally, the contribution around the peak value at 0.2–0.4 s should be improved and the contribution at the head

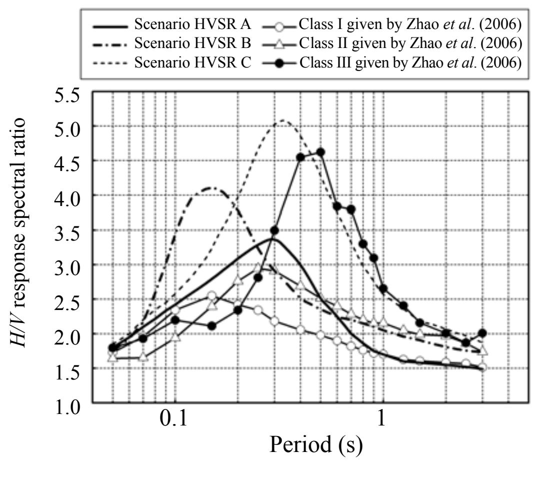

Fig. 2 Scenario HVSRs and standard HVSRs (Zhao *et al*., 2006)

Table 2 SI value of scenario HVSRs

No.	Suggested class	SI				Note
		SC I	SC II	SC III	SC IV	
A	SC II	0.905	0.872	0.748	0.638	Head-tail joggle
B	SC I	0.831	0.901	0.753	0.662	Tail joggle
C	SC II	0.674	0.778	0.882	0.705	Tail joggle

and tail of the curve should be reduced to obtain the best result. A similar situation as tail joggle occurs for Curve B and Curve C. For long periods, the amplification is notable, which matches the standard SC IV curve; thus, the probability of joggle is much less than for the other standard curves. SC II could have either head joggle or tail joggle, resulting in less accuracy, which is consistent with the conclusion from Zhao *et al*. (2006).

2.4 HVSR classification schemes (Ghasemi *et al*., 2009)- Method 3

Ghasemi *et al*. (2009) redesigned SI based on Spearman's rank correlation coefficient (Wolfrom, 1999):

$$\mathrm{SI}_k = 1 - 6\sum_{i=1}^{n} \frac{d_i^2}{n\left(n^2-1\right)} \tag{2}$$

where d_i is the rank difference between each HVSR value for the ith period with respect to the kth site class, and n is the total number of periods. An SI ranging from -1 to 1 is used to measure the correlation between the mean HVSR curve for the site of interest and the standard curves without consideration the frequency distribution, while SI=1 indicates a perfect positive correlation.

3 Improved HVSR based on entropy weight theory-Method 4

3.1 Entropy weight theory

Entropy is a quantitative measure of disorder in a system. The concept comes from thermodynamics, which accounts for the heat energy transfer within a system. Shannon (1948) introduced this mathematical theory in the communication field; besides there are also some applications in earthquake engineering (Harte and Vere-Jones, 2005; Dong *et al*., 1984; Feng and Hong, 2009; Main and Naylor, 2008).

The formula of E is recognized as that of entropy and defined according to statistical mechanics:

$$E = -\sum_{i=1}^{m} p_i \ln p_i \tag{3}$$

where p_i is the probability of a system in the ith state, and m is the numbers of possible states, $0 \le p_i \le 1$, $\sum_{i=1}^{m} p_i = 1$.

Weight assignment defines the relative importance and influence of the input parameters in the final justification. The m sets of the scheme including n indicators are used to assemble the assignment array $\boldsymbol{R}$ based on entropy weight theory. The element r_{ij} of array $\boldsymbol{R}$ represents the evaluation grade for the jth indicator of the ith scheme.

$$\boldsymbol{R} = (r_{ij})_{m\times n} \quad (i=1, 2, \ldots, m; j=1, 2, \ldots, n) \tag{4}$$

If the excellent value is r_j^*, i.e.

$$r_j^* = \begin{cases} \max\limits_i\{r_{ij}\}, & \text{more excellent, larger as } j\text{th index} \\ \min\limits_i\{r_{ij}\}, & \text{more excellent, smaller as } j\text{th index} \end{cases} \tag{5}$$

The normalized assignment array $\boldsymbol{B}$ will be

$$\boldsymbol{B} = (b_{ij})_{m\times n} \quad (i=1, 2, \ldots, m; j=1, 2, \ldots, n) \tag{6}$$

where the element $b_{ij} = r_{ij} / r_j^*$ and it is evident that $0 \le b_{ij} \le 1$. According to this procedure, the entropy of jth indicator is defined

$$E_j = -\sum_{i=1}^{m} f_{ij} \ln f_{ij} \tag{7}$$

where $f_{ij} = \dfrac{b_{ij}}{\sum_{i=1}^{m} b_{ij}}$

In statistics, if an indicator represents greater discrepancy between each respective scheme, it will make more of a contribution in the evaluation system, and its corresponding weight will be higher. If the discrepancy tends to zero, so will the weight. The entropy measures the uncertainty of a distribution and reaches a maximum when the probabilities are uniform. The normalized entropy measurement of the jth indicator is:

$$e_j = \frac{E_j}{E_{\max}} = \frac{E_j}{\ln m} = -\frac{1}{\ln m}\sum_{i=1}^{m} f_{ij} \ln f_{ij} \tag{8}$$

Then the objective weight of jth indicator can be given as:

$$h_j = \frac{1-e_j}{\sum_{j=1}^{n}(1-e_j)} = \frac{1-e_j}{n-\sum_{j=1}^{n} e_j} \tag{9}$$

where $0 \le h_j \le 1$, $\sum_{j=1}^{n} h_j = 1$

Equation (9) states that the indicators with less entropy values have higher levels of information content, and a higher weight is assigned to them.

The decision making also needs to include empirical experience, for which the subjective weight should be considered. Equation (10) is applied to combine the objective weight h_j with the subjective one w_j to evaluate the integrated importance of the jth indicator parameter.

$$\lambda_j = \frac{h_j + w_j}{\sum_{j=1}^{n}(h_j + w_j)} = \frac{h_j + w_j}{1+\sum_{j=1}^{n} w_j} \tag{10}$$

3.2 Procedure of entropy weight evaluation

While the entropy weight of each indicator is involved, the assignment array $\boldsymbol{B}$ will be transferred into $\boldsymbol{A}$, as shown in Eq. (11)

$$\boldsymbol{A} = (a_{ij})_{m\times n} \quad (i=1, 2, \cdots, m; j=1, 2, \cdots, n) \tag{11}$$

where the element $a_{ij} = b_{ij} \times \lambda_j$, and the indicator vector of the ith scheme of the $\boldsymbol{A}$:

$$\boldsymbol{A}_i = (a_{i1}, a_{i2}, \ldots, a_{in}) \tag{12}$$

Calculating the expected assignment of the indicators as

$$\boldsymbol{P} = (p_1, p_2, p_j \ldots, p_n) \tag{13}$$

where p_j denotes the maximum value of jth column in array $\boldsymbol{A}$, as shown

$$p_j = \max_i \{a_{ij} \mid i = 1, 2, \cdots, m\} \quad (j=1, 2, \ldots, n) \tag{14}$$

Then the similarity C_i between vector $\boldsymbol{A}_i$ and vector $\boldsymbol{P}$ is

$$C_i = \frac{\boldsymbol{P} - \boldsymbol{A}_i}{\boldsymbol{P}} = \frac{\boldsymbol{P} \cdot \boldsymbol{P}^{\mathrm{T}} - \boldsymbol{A}_i \cdot \boldsymbol{P}^{\mathrm{T}}}{\boldsymbol{P} \cdot \boldsymbol{P}^{\mathrm{T}}} = \frac{\sum_{j=1}^{n} (p_j)^2 - \sum_{j=1}^{n} (a_{ij} \cdot p_j)}{\sum_{j=1}^{n} (p_j)^2} = 1 - \frac{\sum_{j=1}^{n} (a_{ij} \cdot p_j)}{\sum_{j=1}^{n} (p_j)^2} \tag{15}$$

In the end, the minimum C_i means the best decision with respect to the ith scheme for all of the possible states.

3.3 Test case study

A test case to illustrate the improved HVSR method in solving the "head-tail joggle" issue in Methods 2 and 3 is discussed in this section. Suppose that there are four types of site classification and five indicators, i.e. m=4 and n=5, $r_j^* = \max_i \{r_{ij}\}$ will be set as the expected excellent value. To show the difference between the evaluated values, the following parameters are set: $r_{4j} \geq r_{1j} \geq r_{2j} \geq r_{3j}$, then $r_j^* = r_{4j}$ (j=1, 2, …, 5), $b_{4j} = 1$. And, $b_{3j} = x$, b_{1j}, b_{2j} and b_{3j} are as listed in assignment array $\boldsymbol{B}_{\mathrm{e}}$, see Table 3.

The entropy of each indictors e_j (j=1, 2, …, 5) is calculated and it was found that e_j is a function whose value increases as the variable x increases, and the variation of each indicator decreases. When x reaches maximum, the entropy is the maximum. Meanwhile, the variation of each indicator tends to minimum, especially for j=1; when x=1, the indicators value will be uniform, the variation is zero, and the entropy weight is zero as well.

In addition, for jth indicator, $\sum_{i=1}^{3} (b_{4j} - b_{ij}) = 3 - \sum_{i=1}^{3} b_{ij}$ was used to show the discrepancy between the other indicator values and the maximum one. As shown in Table 3, the difference decreases from j=1 to j=5; however, Fig.3 shows that for a given x, the entropy gradually increases. From this description, there is no doubt that the weight for one indicator in the evaluation system increases following the rise of the difference between its assigned values of all schemes.

Table 3 The assignment array $\boldsymbol{B}_{\mathrm{e}}$ of the test case

Site class	b_{ij}				
	j=1	j=2	j=3	j=4	j=5
I (i =1)	x ($0 \leq x \leq 1$)	$2x$ ($0 \leq x \leq 1/2$)	$2x$ ($0 \leq x \leq 1/2$)	$3x$ ($0 \leq x \leq 1/3$)	$6x$ ($0 \leq x \leq 1/6$)
II (i =2)	x	x	$1.5x$	$2x$	$3x$
III (i =3)	x	x	x	x	x
IV (i =4)	1	1	1	1	1

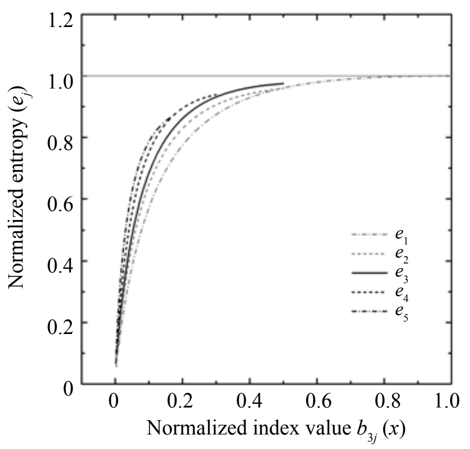

Fig. 3 Entropy vs. value b_{3j}

4 Example case: free-field Station 062WUD

4.1 Description of the Station 062WUD

Based on Entropy weight theory and the index function, the free-field strong motion station in Wudu in Ganshu Province (Code: 062WUD) was selected as an example to analyze the site classification. The 062WUD Station is located on the left bank of the Bailongjiang Terrace, longitude 105.0°E, latitude 33.4°N, and exposed two soil layers. Soil descriptions from top to bottom are as follows:

(1) Clay soil: 0.0–4.5m, brown-yellow, black-grey, occasional distribution of fine gravel, sand, slightly wet, loose.

(2) Clay with silt: below 4.5m, yellow-brown, grey-black, occasional distribution of medium gravel, light density, saturated, medium density below 20m.

The interval shear-wave velocity V_{s}. depth for this station is shown in Fig.4. Note that the borehole only reached 28 m. According to the China Seismic Code (GB 5001-2001), this station may be classified as II or III due to the uncertain overburden thickness (Ministry of Construction and General Administration of Quality Supervision, Inspection and Quarantine, People's Republic of China, 2001). To obtain V_s^{30}, the extrapolation method was used assuming a constant velocity from the ensuing depth to 30m, as the shear-wave velocity should not have much variation at depth (Boore, 2001; Kuo *et al*., 2011). In addition, Kuo *et al*. (2011) examined the accuracy of this method by means of the measured PS-logging data in northeastern Taiwan, and the results showed a low error rate. Thus, the computed V_s^{30} equals 220.9 m/s for the 062WUD Station, and correspondingly, the site was classified as Class D, following the NEHRP site class definition (BSSC, 2003).

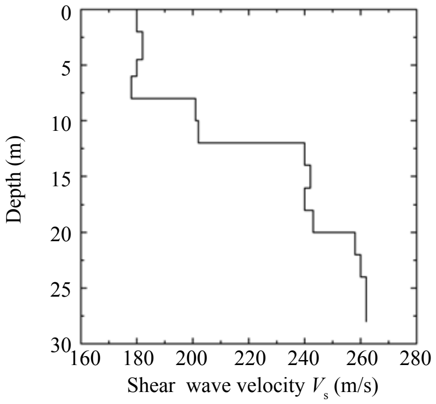

Fig. 4 062WUD station shear wave velocity profile by P-S wave measurement

4.2 Strong motion data of the station

Forty-four sets of strong motion recordings were selected from the Wenchuan aftershocks with magnitudes of M_s3.8–6.5, and their epicenter distribution is shown in Fig.5. The epicenter distance of the 062WUD Station varies from 83.4 km to 268.8 km, as shown in Fig.6, in which the rectangle is the rupture projection on the surface based on finite fault modeling at USGS (http://earthquake.usgs.gov/earthquakes/eqinthenews/2008/us2008ryan/finite_fault.php). A baseline offset for these strong motion data could not be found, so the data processing only includes Butterworth filtering and bandwidths from 0.25 Hz to 25 Hz, which are available for 0.03–3.0 s velocity response spectra calculation.

4.3 Site classification of the station

Following the Zhao *et al*. (2006) HVSR method, the mean response spectra of 5% damped ratio for horizontal ground motion by averaging the natural logarithms can be expressed as:

$$\ln(H) = \frac{\ln g_{EW} + \ln g_{NS}}{2} \tag{16}$$

where H is the average horizontal component, and g_{EW} and g_{NS} are the north-south and east-west components of ground motion, respectively. For all 44 strong motion records, the calculated average HVSRs are shown in Fig.7. Note that two peak periods at 0.2 s and 0.7 s can be observed.

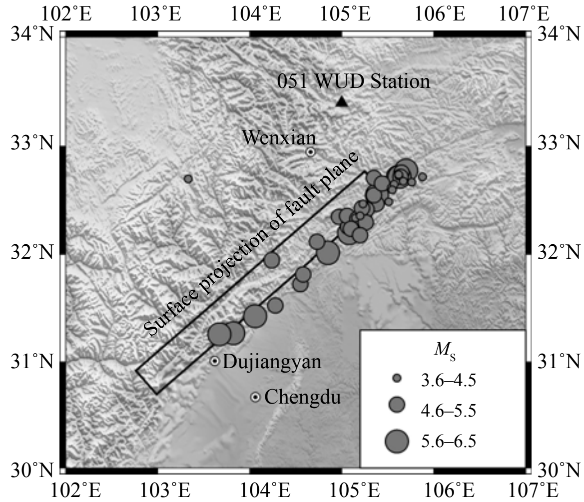

Fig. 5 Epicenters distribution of the aftershocks for 062WUD Station

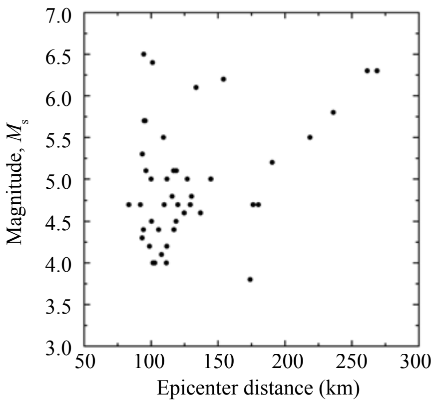

Fig. 6 Magnitudes of the aftershocks vs. epicenter distance for 062WUD Station

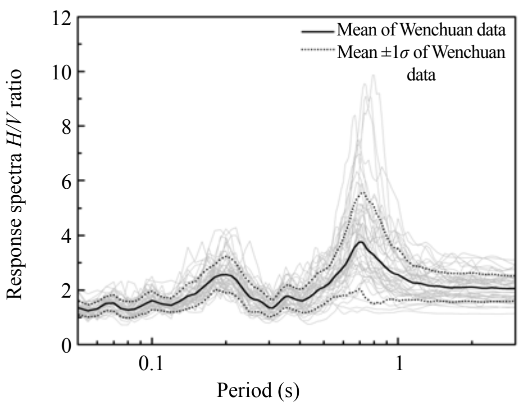

Fig. 7 Average HVSR at 062WUD Station (5% damping)

Then the improved method proposed in this paper is applied to the 062WUD station site classification. The assignment arrays ***R*** and ***B*** are given in Tables 4 and 5. With Eq. (7), Eq. (8), Eq. (9) and Eq. (10), the normalized entropy, objective weight and subjective weight were calculated as shown in Table 6.

For the subjective weight, the following equations

Table 4 Assignment array *R* of the 062WUD Station

Site class	Indictors ***R***, for periods																		
	0.05 s	0.07 s	0.1 s	0.15 s	0.2 s	0.25 s	0.3s	0.4 s	0.5 s	0.6 s	0.7 s	0.8 s	0.9 s	1.0 s	1.25 s	1.5 s	2.0 s	2.5 s	3.0 s
SC I	0.892	0.883	0.832	0.844	0.964	0.855	0.797	0.882	0.964	0.753	0.549	0.62	0.707	0.759	0.822	0.842	0.84	0.844	0.834
SC II	0.912	0.958	0.911	0.874	0.957	0.768	0.708	0.777	0.904	0.892	0.671	0.744	0.833	0.892	0.949	0.959	0.96	0.936	0.905
SC III	0.868	0.883	0.851	0.932	0.944	0.79	0.656	0.626	0.672	0.834	0.994	0.995	0.937	0.978	0.953	0.993	0.97	0.939	0.987
SC IV	0.862	0.919	0.914	1	0.864	0.924	0.838	0.839	0.831	0.883	0.984	0.868	0.805	0.786	0.774	0.808	0.847	0.888	0.895

Table 5 Normalized assignment array *B* of the 062WUD Station

Site class	Indictors ***B***, for periods																		
	0.05 s	0.07 s	0.1 s	0.15 s	0.2 s	0.25 s	0.3s	0.4 s	0.5 s	0.6 s	0.7 s	0.8 s	0.9 s	1.0 s	1.25 s	1.5 s	2.0 s	2.5 s	3.0 s
SC I	0.977	0.922	0.91	0.845	1	0.925	0.951	1	1	0.845	0.552	0.623	0.755	0.776	0.862	0.849	0.866	0.899	0.845
SC II	1	1	0.997	0.874	0.993	0.831	0.845	0.881	0.938	1	0.675	0.748	0.89	0.912	0.996	0.966	0.989	0.997	0.917
SC III	0.952	0.922	0.931	0.932	0.98	0.855	0.783	0.709	0.697	0.935	1	1	1	1	1	1	1	1	1
SC IV	0.945	0.959	1	1	0.896	1	1	0.951	0.862	0.99	0.99	0.873	0.86	0.804	0.812	0.814	0.873	0.946	0.907

Table 6 Normalized entropy and weight ×10[1] of the 062WUD Station

	Indictors, for periods																		
	0.05 s	0.07 s	0.1 s	0.15 s	0.2 s	0.25 s	0.3 s	0.4 s	0.5s	0.6s	0.7s	0.8s	0.9 s	1.0 s	1.25 s	1.5 s	2.0 s	2.5 s	3.0 s
Normalized entropy	9.998	9.996	9.994	9.985	9.993	9.981	9.967	9.942	9.938	9.984	9.781	9.891	9.964	9.963	9.971	9.973	9.984	9.993	9.987
Objective weight	0.025	0.058	0.087	0.213	0.094	0.268	0.46	0.809	0.873	0.219	3.06	1.526	0.502	0.521	0.408	0.372	0.228	0.094	0.182
Subjective weight	0	0	0	1.25	2.5	1.25	0	0	0	1.25	2.5	1.25	0	0	0	0	0	0	0
Total weight	0.013	0.029	0.043	0.732	1.297	0.759	0.23	0.404	0.436	0.734	2.78	1.388	0.251	0.261	0.204	0.186	0.114	0.047	0.091

Table 7 Assignment array *A* subjected to entropy weight ×10[1] of the 062WUD Station

Site class	Indictors, for periods																		
	0.05 s	0.07 s	0.1 s	0.15 s	0.2 s	0.25 s	0.3 s	0.4 s	0.5 s	0.6 s	0.7 s	0.8 s	0.9 s	1.0 s	1.25 s	1.5 s	2.0 s	2.5 s	3.0 s
SC I	0.012	0.027	0.039	0.618	1.297	0.702	0.219	0.404	0.436	0.621	1.534	0.865	0.189	0.202	0.176	0.158	0.099	0.042	0.077
SC II	0.013	0.029	0.043	0.639	1.288	0.631	0.195	0.356	0.409	0.734	1.878	1.038	0.223	0.238	0.203	0.18	0.113	0.047	0.084
SC III	0.012	0.027	0.04	0.681	1.271	0.649	0.18	0.287	0.304	0.687	2.78	1.388	0.251	0.261	0.204	0.186	0.114	0.047	0.091
SC IV	0.012	0.028	0.043	0.732	1.163	0.759	0.23	0.385	0.376	0.727	2.753	1.212	0.216	0.21	0.166	0.151	0.1	0.045	0.083

Table 8 Expected assignment of the indicators ×10[1] of the 062WUD Station

Vector $\boldsymbol{P}_i$																		
p_1	p_2	p_3	p_4	p_5	p_6	p_7	p_8	p_9	p_{10}	p_{11}	p_{12}	p_{13}	p_{14}	p_{15}	p_{16}	p_{17}	p_{18}	p_{19}
0.013	0.029	0.043	0.732	1.297	0.759	0.23	0.404	0.436	0.734	2.78	1.388	0.251	0.261	0.204	0.186	0.114	0.047	0.091

were used:

$$w_j = \begin{cases} \dfrac{1}{4n} & \text{for } (j-1)\text{th and } (j+1)\text{th index} \\ & \text{correspongding to predominant period} \\ \dfrac{1}{2n} & \text{for } j\text{th index correspongding to} \\ & \text{predominant period} \\ 0 & \text{for others} \end{cases} \quad (17)$$

where n is the number of peak periods, for the test case n=2.

The entropy at the 0.7 s and 0.8 s has the minimum value and the maximum objective weight, that match the concept of the improved HVSR in this paper to change uniform weight. Then the updated assignment array $\boldsymbol{A}$ subjected to entropy weight and expected vector $\boldsymbol{P}$ are given in Table 7 and Table 8, respectively. Finally, the similarity C_i between vector $\boldsymbol{A}_i$ and vector $\boldsymbol{P}$ is listed in Table 9 and the value C_3 is the minimum. It is concluded that SC III is the best site classification, which is consistent with the result obtained using the previously determined V_s^{30} parameter.

Table 9 Similarity between A_i and expected vector P of the 062WUD Station

C_1 (SC I)	C_2 (SC II)	C_3 (SC III)	C_4 (SC IV)
0.3262	0.2367	0.0225	0.0420

5 Site classification for NSMONS

5.1 Strong motion data set

In this section, 54 free-field stations including the 062WUD Station, each with more than five recordings, were selected for site classification, as shown in Fig. 8. The strong motion recordings were 383 aftershocks of M_s3.3–M_s6.5 of the Wenchuan earthquake from NSMONS, including 1,982 sets of three-channel strong motion recordings from stations with epicenter distances as shown in Fig. 9. Since the baseline offset for these strong motion data does not include peak ground acceleration, acceleration, velocity and displacement response spectrum (Boore, 2001), the data processing only includes Butterworth filtering, for bandwidths from 0.25 Hz to 25 Hz, which are available for 0.05–3.0 s velocity response spectra calculation.

5.2 Comparisons of classification results by using Methods 1 to 4

Following the site classification procedure used for the 062WUD Station, the average HVSRs of all the other 53 stations were calculated and some typical results are shown in Fig.10. Note that the overall shapes

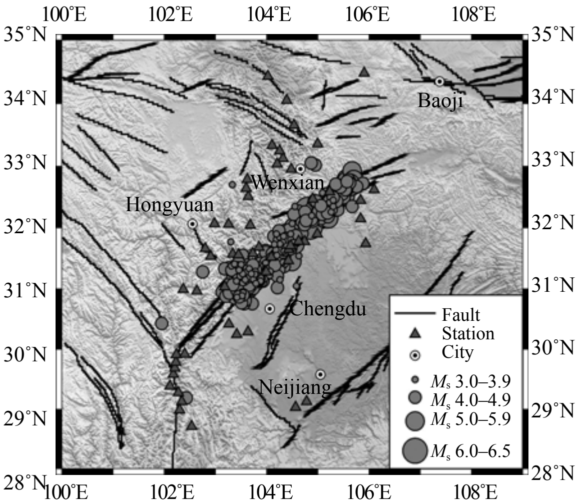

Fig. 8 Distribution of selected free-field stations and the related Wenchuan aftershocks

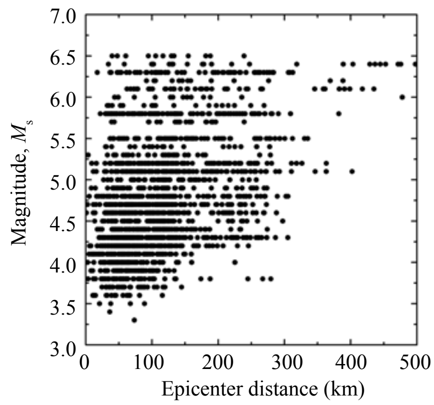

Fig. 9 Magnitude of the aftershocks vs. epicenter distance for all recordings of the NSMONS

and amplitudes of the average *H/V* spectral ratios are remarkably different for different stations. Actually, some stations have only one natural period and it is easy to distinguish it for the one primary soil layer, such as the 051GYS Station (see Fig.10 (a)); some have two natural periods for their two principal soil layers, such as the 051JZW Station (see Fig.10 (b)); for some stations, the peak periods are indistinct due to the complexity of the soil layering, such as the 051CXQ Station (see Fig.10 (c)); and for some stations, the natural period is difficult to identified, since they are located on rock and the *H/V* is close to 1, such as the 062WIX Station (see Fig.10 (d)).

Note that most of the selected NSMONS stations are mainly classified as Class B or Class C, regardless of the methods applied, which is consistent with the geology of the Wenchuan earthquake region. For Method 1, if there are two peak periods, then the larger one is selected as the natural period such as for the 062WUD Station, where T_G=0.71 s, and the site class is E. If two peak values are too close, then the larger one is taken as the natural period such as for the 051JZW Station, where the peak value 3.5 appears at 0.11 s and 0.26 s, so $T_G = 0.26$ s and the site class is C. For HVSR's adjacent to 1 overall, the site class can just be set at Class B. Method 1 has its obvious limitation and uncertainty. Compared with the results from various methodologies, as shown in Table 10, it is seen that the results obtained with Methods 2 and 3 are obviously different, while Methods 3 and 4 are consistent above 70%. All classification results from the four methods are shown in Table 11, and the recommended site classes of all 54 stations are plotted in Fig. 11.

5.3 Discussion

In Section 2.3, an explanation of the head or tail joggle phenomenon was provided and an excellent example is now seen at the 051GYS Station. In Fig. 12, the peak period is 0.12 s and following Method 1, it is attributed to Class B, as is also the case for Methods 3 and 4. For Method 2, the result is Class C, which strongly reflects the tail joggle phenomenon. For periods greater than 0.3 s, the HVSR curve is close to the standard Class

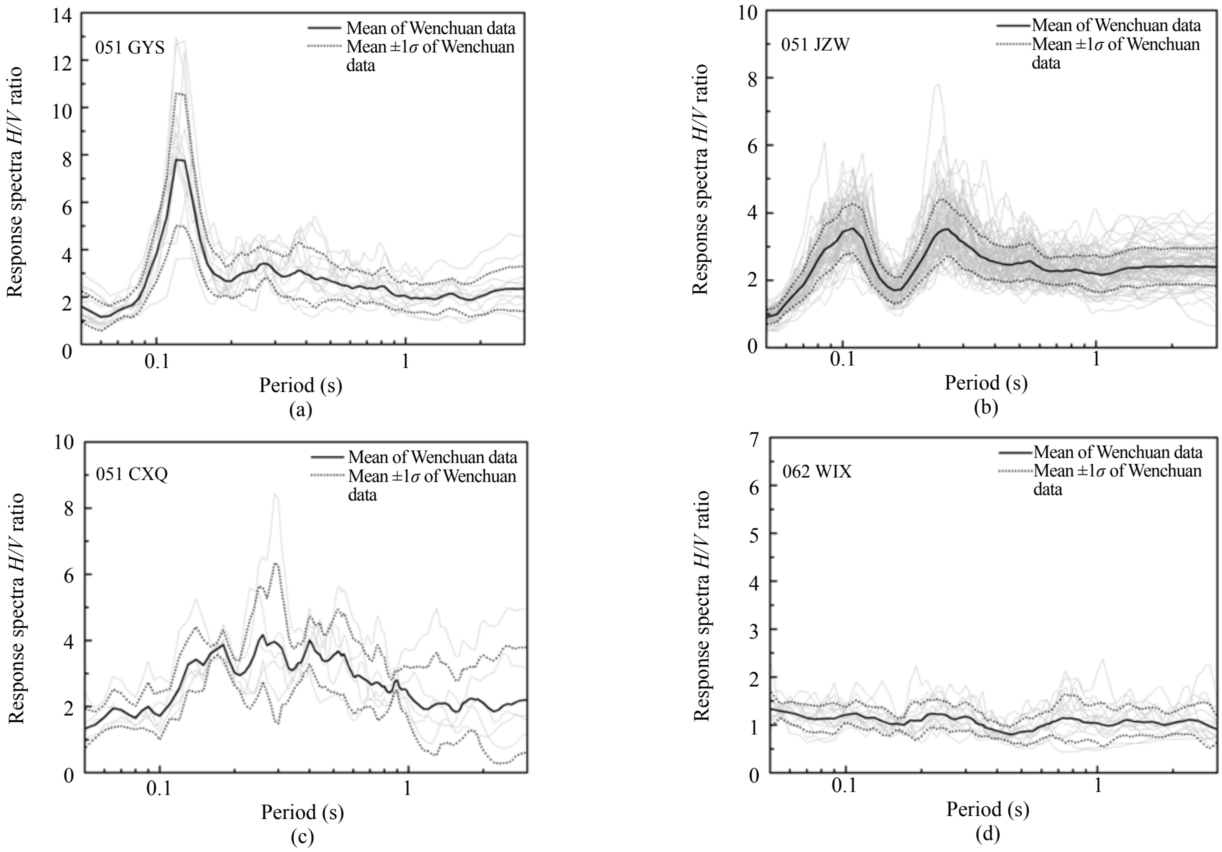

Fig. 10 Typical HVSRs for NSMONS (5% damping)

Table 10 Comparison of the station numbers of site class identified by different methodologies

Identified by M1	Identified by M2				Total	Identified by M1	Identified by M3				Total
	B	C	D	E			B	C	D	E	
B	18	10	3	0	31	B	22	6	2	1	31
C	4	9	1	0	14	C	1	10	3	0	14
D	1	1	1	1	4	D	0	0	2	2	4
E	1	3	1	0	5	E	0	2	1	2	5
Total	24	23	6	1	54	Total	23	18	8	5	54

Identified by M2	Identified by M3				Total	Identified by M3	Identified by M4				Total
	B	C	D	E			B	C	D	E	
B	14	6	3	1	24	B	23	0	0	0	23
C	8	11	1	3	23	C	7	9	1	1	18
D	1	1	4	0	6	D	1	3	4	0	8
E	0	0	0	1	1	E	1	2	2	0	5
Total	23	18	8	5	54	Total	32	14	7	1	54

Note: M1, M2, M3 and M4 denote Methods 1, 2, 3 and 4, respectively

Table 11 Site classes for 54 NSMONS free-field stations

Station name	Lon.(°)	Lat.(°)	Method 1		Method 2	Method 3	Method 4				
			T_G	SC			C_1	C_2	C_3	C_4	SC
051AXB	104.4	31.6	0.180	B	B	B	0.0132	0.0759	0.0932	0.1287	B
051AXT	104.4	31.5	0.620	E	D	D	0.4467	0.3131	0.0206	0.0462	D
051AXY	104.5	31.7	0.085	B	C	B	0.0399	0.1488	0.0950	0.1779	B
051CXQ	105.9	31.7	0.260	C	C	C	0.1266	0.0268	0.0805	0.2289	C
051FSB	104.8	29.1	0.075	B	C	B	0.0068	0.1222	0.0831	0.1515	B
051GYQ	105.8	32.4	0.085	B	B	B	0.0034	0.1383	0.1123	0.1966	B
051GYS	105.8	32.1	0.120	B	C	B	0.0232	0.0956	0.1018	0.1803	B
051GYZ	106.1	32.6	0.250	C	C	C	0.2377	0.0415	0.0432	0.3250	C
051HSD	103.0	32.1	0.080	B	B	B	0.0237	0.1239	0.0651	0.0978	B
051HSL	103.3	32.1	0.270	C	B	C	0.0326	0.0085	0.1149	0.1058	C
051JYC	105.0	31.9	0.140	B	C	B	0.0374	0.0745	0.2063	0.3430	B
051JYD	104.7	31.8	0.130	B	C	B	0.0487	0.0835	0.1803	0.2979	B
051JYH	104.6	31.8	0.075	B	B	B	0.0022	0.1142	0.0876	0.1368	B
051JZB	104.1	33.3	0.350	C	C	C	0.1204	0.0004	0.1744	0.1442	C
051JZG	104.3	33.1	0.200	C	C	C	0.0865	0.0244	0.0933	0.1418	C
051JZW	104.2	33.0	0.11/0.26	B	C	C	0.1116	0.0491	0.0606	0.1802	C
051JZY	104.3	33.2	0.150	B	B	C	0.0129	0.0516	0.1300	0.1849	B
051LDD	102.2	29.6	0.560	D	E	E	0.5182	0.3795	0.0046	0.1262	D
051LDJ	102.2	29.7	0.08/0.29	C	B	D	0.0731	0.0342	0.1047	0.0688	C
051LDL	102.2	29.8	0.1/0.4	D	D	D	0.3967	0.2890	0.0138	0.3346	D
051LDS	102.2	29.9	0.270	C	C	C	0.0276	0.0210	0.1451	0.0760	C
051LXM	103.3	31.6	0.330	C	C	D	0.2118	0.0383	0.0624	0.1816	C
051LXS	102.9	31.5	0.08/0.26	B	B	D	0.0474	0.1046	0.1457	0.0665	B
051LXT	103.4	31.6	-	B	B	B	0.0028	0.1011	0.2193	0.2436	B
051LXY	102.8	31.7	0.1/0.29	B	D	D	0.2066	0.1204	0.0472	0.2441	D
051MXB	103.9	31.7	-	B	B	C	0.0039	0.1143	0.2559	0.2660	B
051MXD	103.7	32.0	0.740	E	B	E	0.0767	0.0238	0.2251	0.2091	C
051MXN	103.7	31.6	0.510	D	B	D	0.0492	0.0431	0.2046	0.1067	C
051MZQ	104.1	31.5	0.150	B	B	B	0.0028	0.0683	0.1128	0.1760	B
051PJD	103.4	30.2	0.340	C	D	D	0.4272	0.2248	0.0052	0.4181	D
051PJW	103.6	30.3	0.310	C	C	C	0.3396	0.1382	0.0121	0.3693	D
051QCD	105.2	32.6	0.110	B	B	B	0.0114	0.1017	0.1053	0.1612	B
051QCQ	104.9	32.5	0.130	B	C	B	0.0214	0.0637	0.1478	0.2322	B
051QLY	103.3	30.4	0.150	B	C	B	0.0336	0.0681	0.1761	0.3019	B
051SFB	104.0	31.3	0.150	B	D	C	0.0712	0.0905	0.2009	0.3385	B
051SMC	102.3	29.1	0.100	B	C	E	0.0150	0.1244	0.0901	0.1516	B
051SMK	102.1	29.4	0.470	D	C	E	0.1339	0.0084	0.1828	0.1326	C
051SML	102.3	29.0	0.270	C	B	B	0.0064	0.0535	0.0692	0.1031	B
051SMX	102.3	29.3	-	B	B	B	0.0024	0.1124	0.2513	0.2669	B
051SPA	103.6	32.5	0.150	B	B	C	0.0057	0.0517	0.1183	0.1816	B
051SPC	103.6	32.8	0.230	C	C	C	0.1007	0.0117	0.0795	0.2019	C
051SPT	103.6	32.6	-	B	B	B	0.0033	0.1101	0.2425	0.2662	B
051TQL	102.4	29.9	0.110	B	C	B	0.0112	0.1504	0.1320	0.2180	B
051WCW	103.2	31.0	0.120	B	D	B	0.0219	0.0757	0.1661	0.2604	B
051XJB	102.4	31.0	-	B	B	B	0.0026	0.1119	0.2511	0.2660	B
051XJD	102.6	31.0	-	B	B	C	0.0028	0.1016	0.2219	0.2413	B
051YBY	104.6	29.0	0.170	B	B	B	0.0317	0.0480	0.1342	0.2324	B
051YXX	102.5	28.7	0.42/1.8	E	C	C	0.2274	0.1821	0.2192	0.1148	E
062MXT	104.0	34.4	0.200	C	C	C	0.1912	0.0086	0.1548	0.3556	C
062SHW	104.5	33.7	0.280	C	B	C	0.0067	0.1069	0.1234	0.0877	B
062TCH	104.4	34.0	0.180	B	B	B	0.0144	0.0538	0.1281	0.2024	B
062TSH	105.9	34.5	0.31/1.15	E	C	C	0.0082	0.1032	0.2107	0.2273	B
062WIX	104.5	32.9	-	B	B	B	0.0025	0.0920	0.1990	0.2335	B
062WUD	105.0	33.4	0.21/0.71	E	C	E	0.3262	0.2367	0.0225	0.0420	D

Note: T_G, the peak period of site; SC, site class; C_i (i=1, 2, 3, 4), similarity of entropy-weight decision theory
"-" of T_G, means that the site has non-existent peak period; "/" of T_G, means that the site has more than one peak period

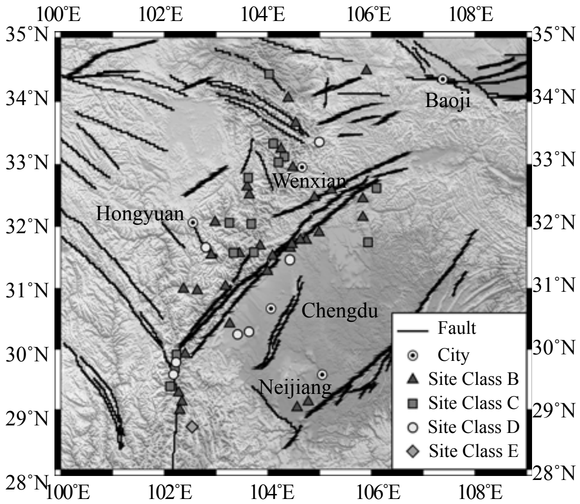

Fig. 11 Suggested site classification for all 54 free field stations

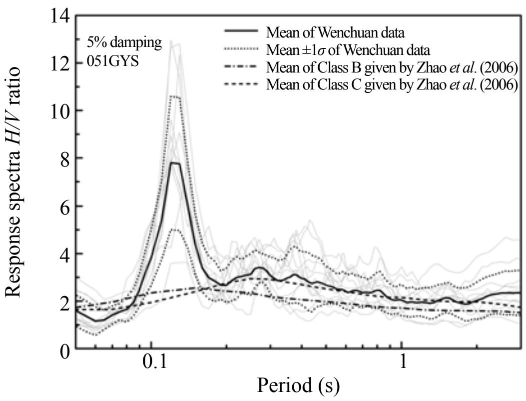

Fig. 12 Tail joggle phenomenon for 051GYS Station by Method 2

C curve given by Zhao *et al*. (2006), which is similar to Curve B in Fig. 2.

Stations 051MXB and 051XJD were installed in a deep hill cave with the accelerometers on stiff rock, site classification of Class B and HVSR amplitude close to 1. Methods 1, 2 and 4 all provide a site class of B, but Method 3 recommends Class C since this method only includes the rank instead of the HVSR value of each period based on Spearman's rank correlation theory. Although the entire segment from 0.05 s to 3.0 s in Fig.13 is much less than the curve for Class C, their HVSR shapes are quite similar to the standard Class C, and their Spearman's rank and correlation coefficient SI reach 0.909 and 0.946, respectively, which is considered to be Class C by Method 3. This is perhaps an explanation for why Method 3 fails.

For all 54 stations, only one is classified as Class E. Its HVSR curve shows that there is a platform at 0.2–0.6 s when the ratio is about 2.5 and there is another peak value of about 3.7 at 1.8 s, so the natural period is taken as 1.8s. It is unusual that there would be such soft soil conditions at an elevation of 1,660 m. The site was investigated and it was found that it was located in

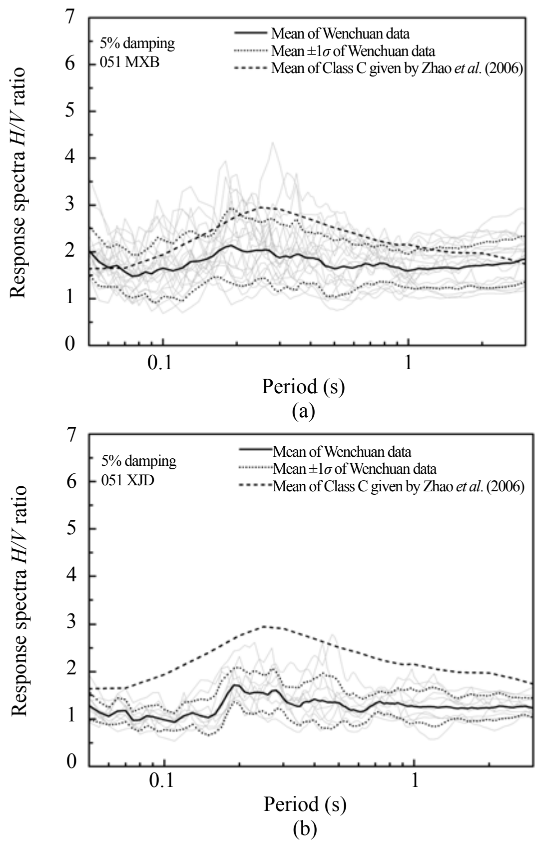

Fig. 13 Mean HVSR for 051MXB and 051XJD Stations and standard Class C curve by Zhao *et al*. (2006)

the Xinmin government yard of Yuexi Country, Sichuan Province. The top overburden is loose backfilled soil, about 70 cm depth, which provides a reasonable explanation for this result.

6 Conclusions

The site classification methodologies for free-field strong motion stations have been summarized in this paper, and the following conclusions can be offered:

(1) Detailed explanations of Method 1 by the HVSR peak period, Method 2 by the HVSR ratio between 0.05–3.0 s, and Method 3 by the HVSR shape were provided and the limitations of each method were discussed.

(2) A new method for site classification was proposed based on the entropy weight theory. The scenario test case study showed that the proposed method avoids the head or tail joggle phenomenon by obtaining the objective and subjective weights.

(3) Based on the entropy weight theory, the station 062WUD was selected as an example to illustrate the procedure of the proposed method. This example supports the concept that the method does change the weight at different periods. By applying the method to the Wenchuan aftershock recordings, the procedure was validated and the result, Class D, shows good agreement with the result given by V_s^{30}.

(4) 54 free-field stations were selected for site classification from NSMONS and their mean *H/V* ratios were calculated using recordings from the Wenchuan aftershocks. The *H/V* curves showed remarkably different amplitudes and shapes for different site classes. Some special site class cases were also analyzed, including the case where HVSR has more than two peak periods and is on soft soil. The results show the improved HVSR in this paper has a better success rate.

The suggested site classifications for NSMONS free-field stations have not yet been accomplished and the Wenchuan earthquake provides an excellent opportunity to test the rationality of the methodology. To verify the availability of this method, a further study will be conducted with data from other destructive earthquakes which have abundant recordings, such as the Tohoku earthquake at March 11, 2011. However, the proposed method may not be suitable for stations that lack adequate strong-motion recordings and it is strongly recommended that drilling tests and PS-logging measurements be used for these other NSMONS stations, and the site classifications can be obtained using the reliable V_s^{30}.

Acknowledgement

The authors appreciate the valuable comments and suggestions provided by the two anonymous reviewers which were used to significantly improve this article. We also thank the China National Strong Motion Network Center for sharing the Wenchuan earthquake strong motion data.

Reference

Bo Jingshan, Qi Wenhao, Liu Hongshuai, Liu Bo, Liu Dedong and Sun Youwei (2009), "Abnormality of Seismic Intensity in Hanyuan During Wenchuan Earthquake," *Journal of Earthquake Engineering and Engineering Vibration*, **29**(6): 53–63. (in Chinese)

Boore DM (2001), "Effect of Baseline Corrections on Displacements and Response Spectra for Several Recordings of the 1999 Chi-Chi, Taiwan," *Bulletin of the Seismological Society of America*, **91**(5): 1199–1211.

Boore DM (2004), "Estimating V_s(30) (or NEHRP Site Classes) from Shallow Velocity Models (Depths < 30 m)," *Bulletin of the Seismological Society of America*, **94**(2): 591–597.

Building Seismic Safety Council (BSSC) (2003), *The 2003 NEHRP Recommended Provisions for New Buildings and Other Structures, Part I* (*Provisions*) *and Part II* (*Commentary*), *FEMA 368/369*, Washington, D.C.

China Earthquake Investigation Group Aboard to Japan (1995), *Investigation of Great Hanshin Earthquake in Japan*, Beijing: Seismological Publishing House. (in Chinese)

Chiou Brian, Darragh Robert, Gregor Nick and Silva Walter (2008), "NGA Project Strong-motion Database," *Earthquake Spectra*, **24**(1): 23–44.

Dong WM, Bao AB and Shan HC (1984), "Use of Maximum Entropy Principle in Earthquake Recurrence Relationships," *Bulletin of the Seismological Society of America*, **74**(2): 725–737.

Feng Lihua and Hong Weihu (2009), "On the Principle of Maximum Entropy and the Risk Analysis of Disaster Loss," *Applied Mathematical Modelling*, **33**(7): 2934–2938.

Fukushima Y, Bonilla LF, Scotti O and Douglas J (2007), "Site Classification Using Horizontal-to-vertical Response Spectral Ratios and Its Impact When Deriving Empirical Ground Motion Prediction Equations," *Journal of Earthquake Engineering*, **11**(5): 712–724.

Gao Zhenhuan and Hu Biru (1987), "The Effect of Local Site Condition on Earthquake Damage Example of Fengrun City in Tangshan Earthquake," *North China Earthquake Sciences*, **5**(Supp.): 208–213. (in Chinese)

Garniel R, Barbui L and Malisan P (2009), "Improvement of HVSR Technique by Self-organizing Map (SOM) Analysis," *Soil Dynamics and Earthquake Engineering*, **29**(6): 1097–1101.

Garniel R, Malisan P, Barazza F and Grimaz S (2008). "Improvement of HVSR Technique by Wavelet Analysis," *Soil Dynamics and Earthquake Engineering*, **28**(4): 321–327.

GEER Association Team (2010). "Geo-engineering Reconnaissance of the 2010 Maule, Chile Earthquake," *GEER Association Report No. GEER-022*.

Ghasemi H, Zare M, Fukushima Y and Sinaeian F (2009), "Applying Empirical Methods in Site Classification, Using Response Spectral Ratio (H/V): A Case Study on Iranian Strong Motion Network (ISMN)," *Soil Dynamics and Earthquake Engineering*, **29**(1): 121–132.

Harte David and Vere-Jones David (2005), "The Entropy Score and Its Uses in Earthquake Forecasting," *Pure and Applied Geophysics*, **162**(6–7): 1229–1253.

Hu YX, Sun PS, Zhang ZY and Tian QW (1980), "Effects of Site Condition on Earthquake Damage and Ground Motion," *Journal of Earthquake Engineering and Engineering Vibration*, **1**(1): 34–41. (in Chinese)

Hwang H, Lin CK, Yeh YT, Cheng CN and Chen KC (2004), "Attenuation Relations of Arias Intensity Based on the Chi-Chi Taiwan Earthquake Data," *Soil Dynamics and Earthquake Engineering*, **24**(7): 509–517.

Japan Road Association (1980), *Specifications for Highway Bridges, Part V*, *Seismic Design*, Maruzen Co., LTD., Tokyo.

Kuo CH, Wen KL, Hsieh HH and Chang TM, Lin CM and Chen CT (2011), "Evaluating Empirical Regression Equations for V_s and Estimating V_s30 in Northeastern

Taiwan," *Soil Dynamics and Earthquake Engineering*, **31**(3): 431–439.

Lee CT, Cheng CT, Liao CW and Tsai YB (2001), "Site Classification of Taiwan Free-Field Strong-motion Stations," *Bulletin of the Seismological Society of America*, **91**(5): 1283–1297.

Lee CT and Tsai BR (2008), "Mapping Vs30 in Taiwan," *Terrestrial Atmospheric and Oceanic Science*s, **19**(6): 671–682.

Li XJ (2009), *Uncorrected Acceleration Records from Fixed Observation for Wenchuan Ms8.0 Aftershocks*, Beijing: Seismological Publishing House, 1–600. (in Chinese)

Li Xiaojun, Zhou Zhenghua, Yu Haiying, Wen Ruizhi, Lu Dawei, Huang Moh, Zhou Yongnian and Cu Jianwen (2008), "Strong Motion Observations and Recordings from The Great Wenchuan Earthquake," *Earthquake Engineering and Engineering Vibration*, **7**(3): 235–246.

Li Zhuofen (1996), "Effect of Site Geology on Earthquake Damage," *Journal of Natural Disasters*, **5**(1): 59–66. (in Chinese)

Lin PS and Lee CT (2008). "Ground-motion Attenuation Relationships for Subduction-zone Earthquakes in Northeastern Taiwan," *Bulletin of the Seismological Society of America*, **98**(1): 220–240.

Liu Shuokuan and Cha Xiaogang (1982), "The Damage Anomaly of 1976 Tangshan Earthquake in High Intensity Region," *Northwestern Seismological Journal*, **4**(2): 67–74. (in Chinese)

Liu KS and Tsai YB (2005), "Attenuation Relationships of Peak Ground Acceleration and Velocity for Crustal Earthquakes in Taiwan," *Bulletin of the Seismological Society of America*, **95**(3): 1045–1058.

Main Ian G and Naylor Mark (2008), "Maximum Entropy Production and Earthquake Dynamics," *Geophysical Research Letters*, **35**: L19311.

Ministry of Construction, People's Republic of China and General Administration of Quality Supervision, Inspection and Quarantine of People's Republic of China (2001), National Standard of People's Republic of China, *Code for Seismic Design of Buildings* (*GB 50011-2001*), Beijing: China Architecture and Building Press.

Nakamura Y (1989), "A Method for Dynamic Characteristics Estimation of Subsurface Using Microtremor on the Ground Surface," *Quarterly Report of the Railway Technical Research Institute*, **30**(1): 25-33.

Ohsaki Y (1969), "The Effects of Local Soil Conditions upon Earthquake Damage," *Proceedings of the Seventh ICSMFE Specialty Session on Soil Dynamics*.

Roumelioti Z and Beresnev IA (2003), "Stochastic Finite-fault Modeling of Ground Motions from The 1999 Chi-Chi, Taiwan, Earthquake: Application to Rock and Soil Sites with Implications for Nonlinear Site Response," *Bulletin of the Seismological Society of America*, **93**(4): 1691–1702.

Seed HB, Romo MP, Sun JI, Jaime A and Lysmer J (1988), "The Mexico Earthquake of September 19, 1985-Relationships Between Soil Conditions and Earthquake Ground Motions," *Earthquake Spectra*, **4**(4): 687–729.

Shannon CE (1948), "A Mathematical Theory of Communication," *Bell System Technical Journal*, **27**: 379–423.

Sokolov VY, Loh CH and Wen KL (2002), "Comparison of the Taiwan Chi-Chi Earthquake Strong-motion Data and Ground-Motion Assessment Based on Spectral Model From Smaller Earthquakes in Taiwan," *Bulletin of the Seismological Society of America*, **92**(5): 1855–1877.

Sokolov VY, Loh CH and Wen KL (2003), "Evaluation of Hard Rock Spectral Models for the Taiwan Region on The Basis of the 1999 Chi-Chi Earthquake Data," *Soil Dynamics and Earthquake Engineering*, **23**(8): 715–735.

Tsai Yi-Ben and Huang Ming-wey (2000), "Strong Ground Motion Characteristics of the Chi-Chi, Taiwan Earthquake of September 21, 1999," *Earthquake Engineering and Engineering Seismology*, **2**(1): 1–21.

Wen Ruizhi, Ren Yefei, Zhou Zhenghua and Shi Dacheng (2010), "Preliminary Site Classification of Free-Field Strong Motion Stations Based on Wenchuan Earthquake Records," *Earthquake Science*, **23**(1):101–110.

Wolfrom S (1999), *The Mathematica Book, Champaign, IL: Wolfrom Media*, Cambridge University Press.

Wood HO (1908), "Distribution of Apparent Intensity in San Francisco," *Report of the State Earthquake Commission*, A.C. Lawson. ed., Carnegie Institute of Washington.

Yamazaki F and Ansary MA (1997), "Horizontal-to-Vertical Spectrum Ratio of Earthquake Ground Motion for Site Characterization," *Earthquake Engineering and Structural Dynamics*, **26**(7): 671–689.

Zare M, Bard PY and Ghafory-Ashtiany M (1999), "Site Characterizations for the Iranian Strong Motion Network," *Soil Dynamics and Earthquake Engineering*, **18**(2): 101–123.

Zhao JX, Irikura K, Zhang J, Fukushima Y, Somerville PG, Asano A, Ohno Y, Oouchi T, Takahashi T and Ogawa H (2006), "An Empirical Site-classification Method for Strong-motion Stations in Japan Using H/V Response Ratio," *Bulletin of the Seismological Society of America*, **96**(3): 914–925.

Zhao JX, Irikura K, Zhang J, Fukushima Y, Somerville PG, Asano A, Saiki T, Okada H and Takahashi T (2004), "Site Classification for Strong Motion Stations in Japan Using H/V Response Spectral Ratio," *13th World Conference of Earthquake Engineering*, Vancouver, B.C., Canada, 1–6 August 2004, Paper No. 1278.

Zhou Xiyuan (1990), *Site Foundation Design Earthquake*, Beijing: Seismological Publishing House. 1–237. (in Chinese)